# Fully Atomistic Molecular Dynamics Simulations of the Behavior of a Simple Model of Crude Oil Confined between Graphene Planes

**E. Maldonado,[†] M. W. Roth,[†,*] and Paul A. Gray[‡]**

Departments of Physics and of Computer Science, University of Northern Iowa, Cedar Falls, Iowa 50614

**ABSTRACT** We present and discuss the results of molecular dynamics computer simulations of crude oil confined between graphene planes. The crude oil is represented as a mixture of alkanes having $6 \leq n \leq 30$ carbons that contain explicit hydrogen atoms; the confining structure is a floor and ceiling, each comprised of graphene sheets. At low temperature, the system adsorbs completely onto the confining layers, showing an interesting domain structure in its own right. As the temperature increases, various species desorb in order of increasing molecular mass and enter the vapor phase between the confining sheets. Desorption proceeds through a roughening of the adsorbed layers but does not appear to couple to any inter- or intramolecular phase transition on the surfaces for any given species. Allowing the graphene sheets to be flexible affects the rate of adsorption as well as the in-plane order and molecular confirmations of the adsorbate. Cursory simulations with more than one layer show droplet-like adsorption at low temperatures and complicated dynamics, which shift the initial desorption temperatures to lower values than those for the monolayer and cause the desorption temperature and process to be much less defined. The results presented here are suggestive of a method of separating alkane mixtures at temperatures significantly different from those of conventional refining processes.

**KEYWORDS:** petroleum • confinement • adsorption • graphene • alkanes

## I. INTRODUCTION

Crude oil and its derivatives are compounds that have deep practical and industrial significance. Although of varying composition, even from the same source, crude oils have distribution spectra of predominantly *n*-alkanes (abbreviated $C_n$), which are straight-chained hydrocarbons having the general formula $C_nH_{2n+2}$. Natural gas is comprised of $C_1-C_5$ molecules in varying ratios (1) and crude oil is generally from $C_6-C_{30}$ (2−7). Some basic practical information about alkanes can be found in Table 1.

Because alkanes comprise a family of compounds, they lend themselves quite nicely to comparative studies in theoretical, computational, and experimental arenas. Because of the wide distribution of alkane chain lengths in crude oils, they make ideal systems for the study of comparisons and contrasts within the alkane family. Computer simulations can give much insight into the behavior of physical systems from both supplementary and predictive standpoints and can shed light on system dynamics not readily accessible in experiments. The studies that exist involving natural gas and crude oil are macroscopic in nature and, although very useful, do not address nanoscale dynamics and processes inside transport pipes and on surfaces. Such an understanding could prove very useful in helping delineate the effects and possible repair of pipe breaks, in facilitating an understanding of new methods of fractionating crude oil and in characterizing the alkane layers adsorbed onto transport pipes that need remediation. In many cases, it then becomes relevant to study the *atomistic* behavior of alkane mixtures in confined geometries.

**Table 1. Basic Information about Various Alkanes**

| compound range | mixture(s) contained in | use |
|---|---|---|
| C1−C4 | natural gas | cooking, heating |
| C5−C10 | naptha and gasoline | solvent chemicals, car fuel |
| C10−C16 | kerosene | heating, jet fuel, lighting |
| C14−C20 | diesel fuels | fuel for trucks/trains |
| C20−C70 | lubricating and fuel oils | machinery, ships, oils, waxes, polishes |
| >C70 | residue/asphaltines | pavement, roofing |

The behavior of atomic and molecular systems in confined geometries has been widely studied (8). Generally, a confined liquid tends to organize into lamellae, or layers. Moreover, there are density and solvation force oscillations perpendicular to the boundary whose wavelength is on the order of the dynamic radius of the confined molecule. Such effects have been studied in confined alkanes (8−16). For organic molecules, branching can disrupt the spatial periodicity of density and solvation force oscillations (17). Another intriguing result is that a confined liquid system can possess a distinctly solidlike character: sheer stress (18). Confinement can also slow down the dynamics of a system and, in particular, longer molecules of a given family can be affected more than shorter ones (18, 19). In addition to the wealth of studies on confined organic systems, computer

* To whom correspondence should be addressed. E-mail: rothm@uni.edu.
Received for review February 10, 2009 and accepted May 14, 2009
† Department of Physics.
‡ Department of Computer Science.
DOI: 10.1021/am900086u

**Table 2. Breakdown of Molecular Composition of the Crude Oil Model Used in This Study**

| species | no. in the simulation box | species | no. in the simulation box |
|---|---|---|---|
| C6 | 20 | C18 | 10 |
| C7 | 21 | C19 | 9 |
| C8 | 25 | C20 | 9 |
| C9 | 26 | C21 | 8 |
| C10 | 23 | C22 | 7 |
| C11 | 20 | C23 | 6 |
| C12 | 17 | C24 | 5 |
| C13 | 17 | C25 | 5 |
| C14 | 15 | C26 | 4 |
| C15 | 15 | C27 | 5 |
| C16 | 12 | C28 | 4 |
| C17 | 11 | C29 | 4 |
| | | C30 | 3 |

simulations have been completed regarding preferential adsorption from mixed-alkane systems (20, 21), thermal desorption of alkanes from a graphite surface (22), adsorption onto graphite from a fluid (23), and odd-alkane impurities in even alkane monolayers (24).

The purpose of this work is to deterministically simulate a simple model of crude oil confined by an emerging nanoscale carbon system: graphene sheets. Specifically, we seek (i) to study the desorption behavior of the system, examine the composition of the gas phase between the graphene planes, and compare the results to standard refining fractionation temperatures, (ii) to understand the dynamics of desorption and the general character of the adsorbed layers, and (iii) to illustrate the effects of allowing the graphene sheets to deform as well as varying the amount of oil placed between the sheets. Because the molecules that desorb are in the gas phase and also because the period of density oscillations of confined liquids depends on the molecular size, this work neither observes nor focuses on oscillatory effects produced by confinement.

## II. COMPUTATIONAL METHOD

**A. Simulation Details.** Because crude oil contains a smaller percentage of longer alkanes and also because of the explicit hydrogen model of the alkanes in the simulations presented here, it is necessary to have fairly large systems, which, in turn, implies the need for a significant amount of computational time. Because of this, we chose a molecular dynamics simulation package with massively parallel capability: NAMD (25). NAMD is a freely available parallel molecular dynamics package that is widely used in the computational modeling of large, usually organic systems (25, 26).

The first task was to determine the molecular composition of the natural gas and crude oil mixtures. Although such mixtures are very complex on the nanoscale, they can be reasonably approximated as containing various proportions of *n*-alkanes, as summarized in Table 2. The oil composition was calculated from relative mass percentages from typical well samples (7). Because gauche defects are supported in the system (oftentimes approximating cyclic geometry, especially by longer molecules) and also because there are relatively fewer aromatics than aliphatics in crude oils, cyclic compounds are omitted in this study.

The preliminary simulations discussed here begin with an oil mixture consisting of alkanes of various lengths as shown in Table 2 placed between two graphene sheets spaced 200 Å apart. The graphene sheets are modeled as being static for the bulk of the simulations done but are also allowed to flex for part of the study. The alkane mixture is in the computational cell such that no part of a molecule is closer than 4 Å to the graphene sheet. Moreover, a UNIX script was created that constructs the Protein Data Bank (27) initial condition file. It places the correct number of molecules in the box starting with the longest (the one with the most carbon atoms), initially having random center-of-mass positions and orientational angles and ensuring that no two atoms of different molecules are closer together than 4 Å. The simulation proceeds with a velocity-rescaling thermostat and a time step of 1 fs, and pair interactions are cut off at a 15 Å separation. The initial configuration was allowed to relax for approximately 5 ns before production runs were carried out for the following 6 ns. At lower temperatures, droplets would form early in the relaxation process that would ultimately be adsorbed by a graphene sheet in the course of the remainder of the relaxation. The initial configuration and a floating droplet early in the system's relaxation are shown in Figure 1.

Furthermore, it is important to track the effects of changes in the various elements of the simulations presented here, and so runs were done where the graphene sheets were allowed to deform and also a series was completed with 4 times the number of molecules as those shown in Table 1, which resulted in greater than monolayer coverage on the graphene sheets.

**B. Interaction Potentials.** All atom−atom interactions in the simulations presented here are in the standard CHARMM22 format (28). There are three types of internal (bonded) interactions between atoms within the same molecule and two types of nonbond interactions between atom pairs. All interactions used in the simulations presented here are summarized in Table 3, and more details about the potential interactions and parameters are found elsewhere (28).

In addition to the interactions mentioned above, there are scaled nonbonded interactions between atoms of the same molecule. Specifically, scaling the nonbonded interactions impacts the intramolecular nonbonded van der Waals energies as well as the Coulomb electrostatic potentials. For the simulations presented here, such interactions for 1−3 pairs (first through third neighbors on the same molecule) are not included, and those for 1−5 and beyond are fully included. However, within NAMD, one can scale the 1−4 interactions and thereby can control the stiffness of the flexible molecules (29, 30). Many simulations employ a value of the scaling factor (SF) = 0.4, but a molecular dynamics study (30) shows that the optimal scaling factor has different values for different alkane chain lengths. In this work, we use SF = 0.4 because it is widely used and also it is not clear as to how the SF issue can be resolved for a mixture of alkanes of varying lengths, vis-à-vis mapping results on a surface (30) to the vapor.

The interactions discussed above apply to oil molecules as well as graphene sheets when the latter is allowed to flex, but in the case of rigid graphene, the only oil−graphene forces on the alkane molecules considered are from the static graphene atoms.

## III. RESULTS AND DISCUSSION

Figure 2 shows final snapshots of the system at various temperatures, and Figure 3 shows the density profile of the system at various temperatures. At the lowest temperatures (below ca. 400 K), the oil forms an adsorbed film on the graphene floor and ceiling, as seen in the snapshots as well as the two strong peaks at either end of the density distribu-

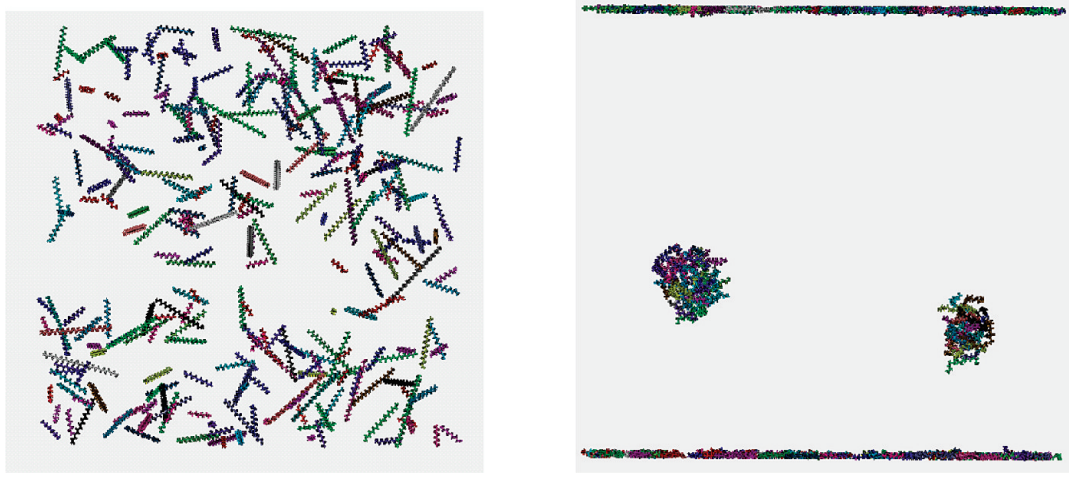

**FIGURE 1. Initial configuration (left) and floating droplets early in the relaxation (right) for a low-temperature system. Molecules are colored based on their species type.**

**Table 3. Expressions for the Types of Interaction Potentials Used in This Work[a]**

| interaction potential | type | formula |
|---|---|---|
| bond stretching | intra, bonded, two-body | $u_{stretch} = k(l - l_0)^2$ |
| bond-angle bending | intra, bonded, three-body | $u_{bend}(\theta) = k_\theta(\theta - \theta_0)^2$ |
| dihedral torsion | intra, bonded, four-body | $u_{dihed} = k_d[1 + \cos(n\phi_d - \delta)]$ |
| van der Waals (modified Lennard-Jones) | inter, nonbonded, two-body | $u_{LJ}(r_{ij}) = \varepsilon_{ij}[(r_0/r_{ij})^{12} - 2(r_0/r_{ij})^6]$ |
| Coulomb (electroscatic) | inter, nonbonded, two-body | $u_C = kq_iq_j/r_{ij}$ |
| scaled nonbonded (Coulomb and van der Waals) | intra, nonbonded | excluded for 1−3 pairs, scaled for 1−4 pairs, and fully included for 1−5 and more distant pairs |

[a] Interactions between atoms on the same molecule are classified as "intra", and those between atoms on different molecules or alkane−graphene interactions are tagged as "inter".

tion. As the temperature increases to about 450 K, the adsorbed layer begins depleting and feeds into the vapor, starting with hexane, the lightest and most mobile oil component. As the temperature increases further, the adsorbed layers continue to feed the vapor phase, and examination of the snapshots suggests that the vapor is comprised of increasingly massive molecules with increasing temperature. Such a progression is confirmed by the molecule fraction and number curves shown in Figure 4. Curves for increasing temperature have increasing height on the graphs, and so the point where the curve intersects the abscissa illustrates the longest carbon chain (molecule with the most carbon atoms) present in the vapor phase. It is interesting to note that above about $T = 700$ K the component with the greatest fraction as well as the number of vapor changes from hexane (C6) to decane (C10). Such an effect may be due to steric hindrance from longer molecules in the vapor because above $T = 700$ K the curves in Figure 4 lift considerably for C24 and above, indicating their increased presence in the vapor. Even though alkanes lose stability at temperatures above $T = 1000$ K, points at $T = 1100$ and 1200 K are included in order to continue trends set at low temperatures but also to test the limits of NMAD and the CHARMM22 force field.

Figure 5 shows the longest alkane present (molecule with the most carbon atoms) in the vapor at a given temperature. The fractionation temperatures reported here are significantly higher than those for conventional refining distillation techniques (7). It should be noted, however, that we retain a considerable vapor pressure at higher temperatures, and continual removal of desorbed molecules from the vapor could lower desorption temperatures, especially for longer species.

Inspection of the snapshots in Figure 2 as well as internal bond and dihedral angle distributions not shown here suggests that, in concert with desorption, the adsorbed layer roughens, with all or part of some molecules orienting the plane of their backbone away from, being parallel to, the graphene surface. Such dynamics are also evidenced by skewing of the base of the adsorption peaks in the density distributions shown in Figure 3. The average molecule lengths as a function of the temperature shown in Figure 6 are useful indicators of the degree to which molecular flexibility vis-à-vis gauche defects couples to desorption. It is evident that the most rapid change in molecular shape occurs well after a species' desorption temperature is reached, suggesting that the molecules do not need to undergo a chain melting transition on the surface (and become globular) in order to desorb. Rather, as seen in Figure 2, the desorbing molecules tend to leave the surface incrementally; the cost of the whole molecule leaving, especially for longer molecules, is quite large. Once they are in the vapor phase, it is much easier for them to contort through gauche defects. The temperature range where the molecule lengths change the most then correspond to the population of the vapor phase, but any signature of predesorption dynamics in the average molecule length seems to be absent because desorption does not happen for all molecules of a given species at once, as a chain melting transition would.

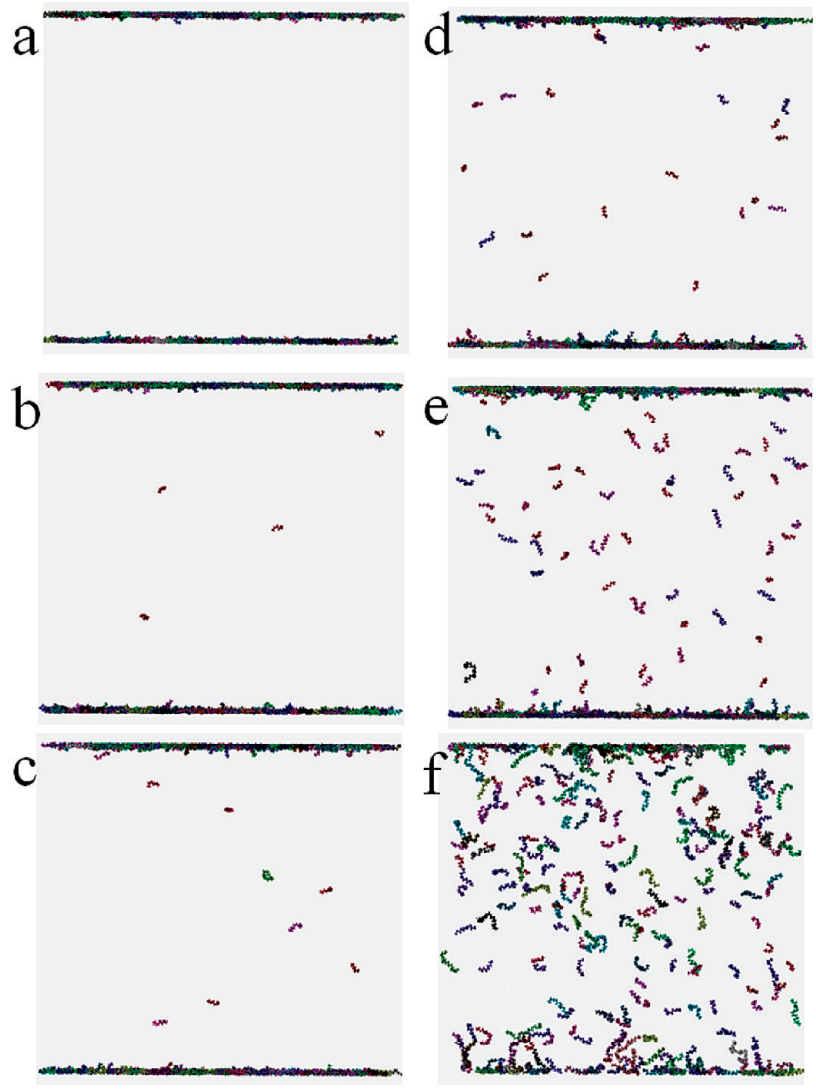


FIGURE 2. Final snapshots of the system at $T = 350$, 450K, 500, 600, 700, and 1200 K (a−f, respectively). Temperature intervals are chosen in order to give a visual appreciation for the changes that the system undergoes with increasing temperature.

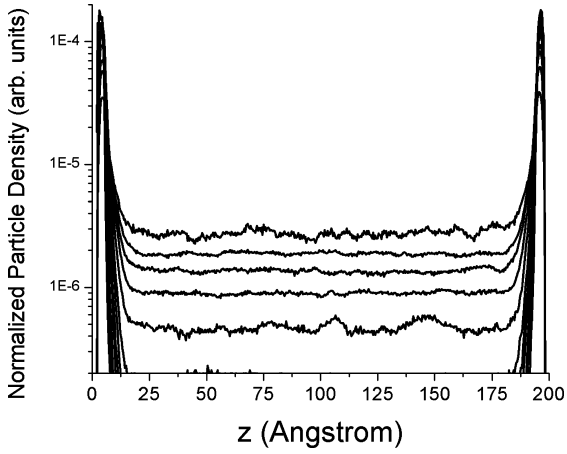


FIGURE 3. Axial density profiles for the system at $T = 450$ K (bottom line with fluctuations barely visible), 500 K (lowest vapor plateau), 600 K, 700 K, 800 K, and 1200 K (highest vapor plateau).

Inspection of snapshots of the adsorbed layer in Figure 7 confirms that there is no global chain melting transition that corresponds to the onset of desorption for any species. The static disorder present is reminiscent of those created by sublattice protrusion seen in earlier simulations created by odd-alkane impurities placed in a host monolayer of even alkanes (24). However, it is interesting to note the presence of an ordered phase at low temperature, which presents a complicated domain-structured fluid in equilibrium with a vapor comprised of smaller molecules in the simulation. Because the translational order of the adsorbed system disappears by $T = 500$ K, it seems that the surface phase (behavior governed by nonbonded interactions) has little to do with desorption as well.

The first type of variation performed was to allow the graphene to deform. Figure 8 shows a typical sequence where the sheet is rippled, much like when one dusts a carpet. When the graphene deforms, there is enough of a disturbance in the adsorbed layer to cause significant surface reordering but not to promote desorption. Moreover, inspection of animation sequences and temporal adsorption data (not shown here) reveals that there are instances where a molecule probably would have adsorbed onto a flat static graphine sheet, but the rippling caused the molecule to bounce, delaying desorption. We interpret such results to

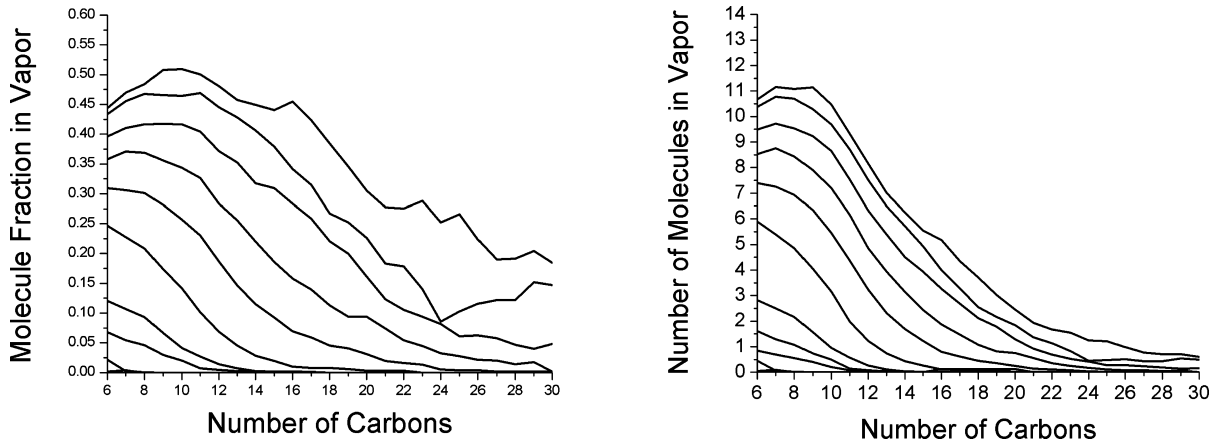


FIGURE 4. Fraction of molecules (left panel) and number of molecules (right panel) in the vapor between the adsorbed layers. The lowest curves (not visible) start at $T = 250$ K; the lowest visible curves are at $T = 450$ K, and the highest curves are at $T = 1200$ K.

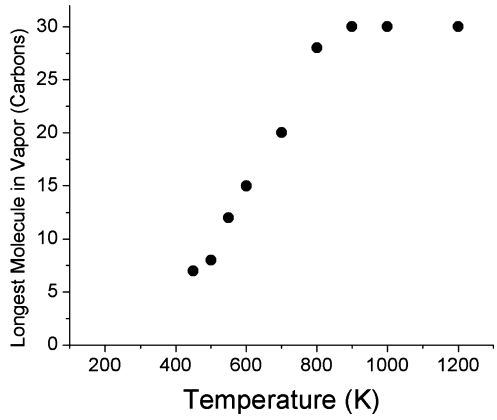


FIGURE 5. Longest molecule present in the vapor (molecule with the most carbon atoms) as a function of the temperature. Points for the lowest three temperatures are not plotted because there could be desorption for molecules lighter than hexane not included in the simulations here and they could provide a visual miscue.

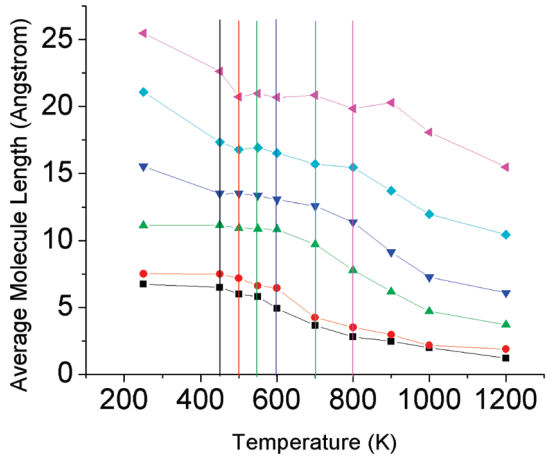


FIGURE 6. Average molecule lengths as a function of the temperature for C7, C8, C12, C15, C20, and C28 (bottom to top). The vertical lines are taken from the data in Figure 5, and the line and curve colors correspond. The lines show the temperature at which the corresponding molecule length is the longest species present (species with the most carbon atoms), suggesting that the species has just begun to desorb with increasing temperature.

mean that dynamic graphene sheets slow adsorption rates slightly and cause significant surface reordering in the adsorbed layer but do not appreciably alter the composition of the desorbed vapor at a given temperature. Because the vibration of a graphene sheet depends on its size and boundary conditions, it would be desirable to systematically study the effects of dynamic graphene for this systems in this work. In addition, the degree of surface rearrangement suggests that variation of the structure of dynamic substrates would not affect the desorption behavior significantly but the laterally averaged holding potential would.

Second, a set of cursory simulations were completed with static graphene sheets and contained 4 times the number of molecules as the simulations described above. This allowed an overlayer to adsorb onto the alkane-coated graphene sheets. The system presented a complicated domain structure similar to those seen in Figure 7, and the second layer tended to take the form of globular droplets, although there were small domains with second-layer molecules parallel to the surface. Because the boundary conditions for the second layer are so different from those of the first layer, the molecules are much more mobile and also exhibit a greater number of defects, which cooperate to cause them to desorb at lower temperatures. Hence, the desorption temperature for a given species is well below that for the monolayer and, with the second layer's dynamics being so different from those of the first desorption, becomes a much less defined phenomenon. It would prove interesting to study the desorption behavior of this system as it transitions from the monolayer toward the bulk.

There are several conclusions that can be drawn from this work: (i) For the bulk of simulations conducted at low density, adsorption from droplets at low temperature results in a flat adlayer with a rich domain structure. (ii) As the temperature increases, molecules leave the graphene surface in order of increasing mobility. (iii) Fractionation temperatures in the low-density case are significantly higher than those for standard refining temperatures. (iv) Allowing the graphene sheets to deform results in surface reorganization and slightly reduced adsorption rates but does not significantly promote or stifle desorption. (v) For higher densities resulting in greater than monolayer coverages, adsorption from droplets at low temperature results in globular-shaped patches. (vi) For the high-density runs, the

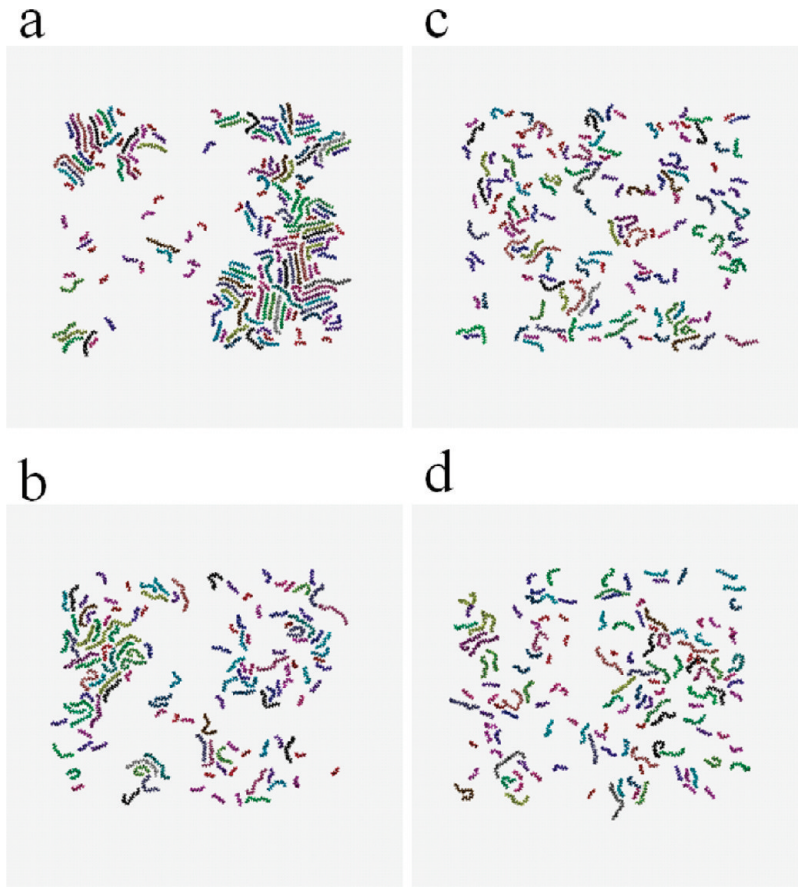


FIGURE 7. Final snapshots of the adsorbed layer at $T = 250$, 300, 400, and 500 K (a−d, respectively).

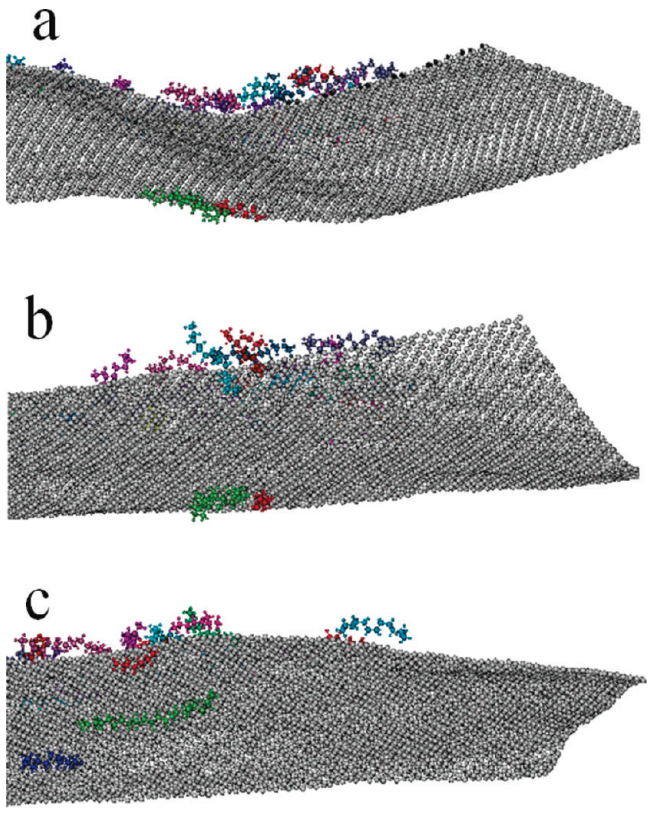


FIGURE 8. Snapshots of the system 1000 ps apart, showing the effect of allowing the graphene to be dynamic. The molecules on the surface reorient but are not thrown off.

dynamics of the adsorbed molecules was more pronounced the farther away they were from the surface, resulting in a blurring of the desorption temperature and behavior seen at lower densities. (vii) Further systematic studies are warranted, such as how the size and shape of the graphene sheets affect the system's behavior, how varying the number of molecules in the simulation affects the results, how varying the nonbonded SF affects the bulk gas or liquid, and how adding molecules of various shapes, for example, cyclic compounds, affects the results.

Generally, crude oil adsorbed onto a surface such as graphene presents a very interesting system where fractionation, if ever practical, would proceed much differently than that for conventional crude oil refining. There is much more computational work to be conducted, not only toward a better understanding of the desorption dynamics but also in characterizing the adsorbed layers.

**Acknowledgment.** The authors gratefully acknowledge support for this work from Petroleum Research Fund Grant PRF43277-B5, as well as a PRF SUMR scholarship for E.M. M.W.R. also acknowledges useful discussions with Christopher Smelker (ChevronPhillips Chemical Co, LP). All of the authors gratefully acknowledge the constructive comments of the reviewers.

## REFERENCES AND NOTES

(1) http://science.jrank.org/pages/4569/Natural-Gas.html.
(2) Hughey, C. A.; Rodgers, R. P.; Marshall, A. G. *Anal. Chem.* **2002**, *74*, 4145.

(3) Sugiura, K.; Ishihara, M.; Shimauchi, T.; Harayama, S. *Environ. Sci. Technol.* **1997**, *31*, 45.
(4) Mutelet, F.; Ekulu, G.; Rogalski, M. *J. Chromatogr., Ser. A* **2002**, *969*, 207 (Sept).
(5) Ha, Z.; Ring, Z.; Liu, S. *Energy Fuels* **2005**, *19*, 1660.
(6) Thanh, N.; Hsieh, M.; Philp, R. P. *Org. Geochem.* **1999**, *30*, 119.
(7) Villalanti, D. C.; Raia, J. C.; Maynard, J. B. In *Encyclopedia of Analytical Chemistry*; Meyers, R. A., Ed.; John Wiley & Sons Ltd.: Chichester, U.K., 2000; p 6726.
(8) Gao, J.; Luedtke, W. D.; Landman, U. *J. Chem. Phys.* **1997**, *106, 10*, 4309, and references cited therein.
(9) Walley, K. P.; Schweizer, K. S.; Peanasky, J.; Cai, L.; Granick, S. *J. Chem. Phys.* **1994**, *100*, 3361.
(10) Jee-Ching, W.; Fichthorn, K. A. *J. Chem. Phys.* **2002**, *116*, 410.
(11) Christenson, H. K.; Gruen, D. W. R.; Horn, R. G.; Israelachvili, J. N. *J. Chem. Phys.* **1987**, *87*, 1834.
(12) Ribarsky, M. W.; Landman, U. *J. Chem. Phys.* **1992**, *97*, 1937.
(13) Landman, U.; Luedtke, W. D.; Ouyang, J.; Xia, T. K. *Jpn. J. Appl. Phys.* **1993**, *32*, 1444.
(14) Gupta, S.; Koopman, D. C.; Westerman-Clark, G. B.; Bitsanis, I. A. *J. Chem. Phys.* **1994**, *100*, 8444.
(15) Manias, E.; Hadziioannou, G.; ten Brinke, G. *Langmuir* **1996**, *12*, 4587.
(16) Winkler, R. G.; Gerstmair, A.; Reineker, P.; Matsuda, T.; Yoon, D. Y. *Phys. Chem. Chem. Phys.* **2001**, *3*, 1155.
(17) Granick, S.; Demirel, A. L.; Cai, L. L.; Peanasky, J. *Isr. J. Chem.* **1995**, *35*, 75.
(18) Klein, J.; Kumacheva, E. *Science* **1995**, *269*, 816.
(19) Granick, S. *Science* **1991**, *253*, 1374.
(20) Xia, T. K.; Landman, U. *Science* **1993**, *261* (5126), 1310.
(21) Hentschke, R.; Schürmann, B. L.; Rabe, J. P. *J. Chem. Phys.* **1992**, *96*, 6213.
(22) Becker, K. E.; Fichthorn, K. A. *J. Chem. Phys.* **2006**, *125*, 184706 DOI.
(23) Hentschke, R.; Winkler, R. G. *J. Chem. Phys.* **1993**, *99*, 5528.
(24) Pint, C. L.; Roth, M. W. *Phys. Rev. B* **2006**, *73*, 115404.
(25) Kale, L. *J. Comput. Phys.* **1999**, *151*, 283. See also http://www.ks.uiuc.edu/Research/namd/.
(26) Jha, S.; Coveney, P. V.; Laughton, C. A. *J. Comput. Chem.* **2005**, *26*, 1617.
(27) Benz, R. W.; Castro-Román, F.; Tobias, D. J.; White, S. H. *Biophys. J.* **2005**, *88*, 805. See also http://www.wwpdb.org/.
(28) Brooks, B. R.; Bruccoleri, R. E.; Olafson, B. D.; States, D. J.; States, S.; Swaminathan, S.; Karplus, M. *J. Comput. Chem.* **1983**, *4*, 187. See also http://www.charmm.org.
(29) Firlej, L.; Kuchta, B.; Roth, M. W.; Connolly, M. J.; Wexler, C. *Langmuir* **2008**, *24*, 12392.
(30) Firlej, L.; Kuchta, B.; Roth, M. W.; Connolly, M. J.; Wexler, C. *J. Chem. Theor. Comput.* **2009**, submitted for publication.

AM900086U